RSC Advances

PAPER

View Article Online
View Journal | View Issue

Cite this: *RSC Adv.*, 2015, **5**, 49287

Ordered mesoporous crystalline aluminas from self-assembly of ABC triblock terpolymer–butanol–alumina sols†

Kwan Wee Tan,[a] Hiroaki Sai,[a] Spencer W. Robbins,[ab] Jörg G. Werner,[ab] Tobias N. Hoheisel,[a] Sarah A. Hesse,[ab] Peter A. Beaucage,[a] Francis J. DiSalvo,[b] Sol M. Gruner,[cd] Martin Murtagh[a] and Ulrich Wiesner*[a]

Received 23rd April 2015
Accepted 28th May 2015

DOI: 10.1039/c5ra07421e

www.rsc.org/advances

A one-pot synthesis approach is described to generate ordered mesoporous crystalline γ-alumina–carbon composites and ordered mesoporous crystalline γ-alumina materials *via* the combination of soft and hard-templating chemistries using block copolymers as soft structure-directing agents. Periodically ordered alumina hybrid mesostructures were generated by self-assembly of a poly(isoprene)-*block*-poly(styrene)-*block*-poly(ethylene oxide) terpolymer, *n*-butanol and aluminum tri-*sec*-butoxide derived sols in organic solvents. The triblock terpolymer was converted into a rigid carbon framework during thermal annealing under nitrogen to support and preserve the ordered mesoporous crystalline γ-alumina–carbon composite structures up to 1200 °C. The carbon matrix was subsequently removed in a second heat treatment in air to obtain ordered mesoporous crystalline γ-alumina structures. Such thermally stable, highly crystalline, and periodically ordered mesoporous ceramic and ceramic–carbon composite materials may be promising candidates for various high temperature catalysis, separation, and energy-related applications.

Introduction

Porous crystalline alumina (Al_2O_3) materials exhibiting high thermal and hydrolytic stability are of interest for various industrial and environmental applications, ranging from membrane filtration, high-temperature absorbers to catalytic supports.[1] In particular, ordered mesoporous crystalline γ-Al_2O_3 structures with high surface area and crystallinity, as well as controlled porosity are highly desirable for high-temperature, size-selective catalytic applications.[1–4] γ-Al_2O_3 prepared by heating boehmite gels (AlOOH) from 400 to 700 °C to induce dehydration and crystallization have excellent textural properties (surface area ~250 $m^2\ g^{-1}$; pore volume ~0.5 $cm^3\ g^{-1}$) but broad pore size distributions.[2,4,5] Above 900 °C, boehmite derived γ-Al_2O_3 transforms into other crystalline phases (δ-, θ-, α-phases),[5] resulting in the loss of surface area and porosity.

Surfactant and block copolymer self-assembly provide a direct pathway to form silica and metal oxide composite materials with tunable mesopore size and periodic morphologies.[1–4,6–34] Yet in many cases, the rapid Al_2O_3 sol–gel hydrolysis reactions disrupted the self-assembly process and resulted in disordered wormlike Al_2O_3 mesostructures that could impede mass transport.[1–4,6,7,11,27,29] The key to achieve periodically ordered mesoporous γ-Al_2O_3 structures *via* block copolymer soft-templating is to control the kinetics of Al_2O_3 sol–gel hydrolysis reactions.[17,21] Yan and co-workers first demonstrated the formation of periodically ordered γ-Al_2O_3 mesostructures by evaporation-induced self-assembly of structure-directing poly(ethylene oxide)-*block*-poly(propylene oxide)-*block*-poly(ethylene oxide) (PEO-*b*-PPO-*b*-PEO) triblock copolymers and Al_2O_3 sol precursors with controlled hydrolysis rates.[21] An alternative route to fabricate mesoporous γ-Al_2O_3 is by backfilling Al_2O_3 sol–gel precursors into hard silica or carbon mesostructured templates, followed by thermal annealing and template removal.[12,18,23] However, the hard templating approach increases both production time and cost due to the addition of tedious processing steps, such as separate preparation of the hard templates and multiple backfilling cycles of the precursors.

Several techniques have recently been devised to maintain porosity and improve thermal stability of mesoporous Al_2O_3 structures, including enhancement of Al_2O_3 sol–gel condensation rates,[3,29] as well as separate addition of metal oxide

[a]*Department of Materials Science and Engineering, Cornell University, Ithaca, New York 14853, USA. E-mail: ubw1@cornell.edu*

[b]*Department of Chemistry and Chemical Biology, Cornell University, Ithaca, New York 14853, USA*

[c]*Department of Physics, Cornell University, Ithaca, New York 14853, USA*

[d]*Cornell High Energy Synchrotron Source, Cornell University, Ithaca, New York 14853, USA*

† Electronic supplementary information (ESI) available: Additional X-ray scattering and electron microscopy characterization of ISO–Al_2O_3 hybrids, mesoporous crystalline Al_2O_3–carbon composites and mesoporous crystalline Al_2O_3 samples. See DOI: 10.1039/c5ra07421e

stabilizers[11,22] and carbon precursors.[5,24] However, ordered mesoporous γ-Al_2O_3 structures and Al_2O_3 based composites typically exhibit thermal stability only up to 1000 °C and collapse at higher temperatures due to sintering of crystalline domains and phase transformations.[4,10,12,15,16,18,19,21–26] Moreover, the small molar mass of structure-directing agents used to date severely limits the accessible pore size of ordered mesoporous crystalline Al_2O_3 structures to less than 10 nm.[1–4,11,17,18,21–25,29]

Previously, we described a facile one-pot synthesis method referred to as the combined assembly by soft and hard (CASH) chemistries to synthesize highly crystalline, ordered mesoporous transition metal oxide structures.[20] Amphiphilic poly(isoprene)-*block*-poly(ethylene oxide) (PI-*b*-PEO) diblock copolymers were employed to structure-direct titania and niobia sols into inverse hexagonal mesostructures. Upon heating in an inert environment, part of the sp^2-hybridized carbon in the hydrophobic PI block converted *in situ* into a rigid carbon matrix (*i.e.*, without additional carbon precursors) that supported the structural integrity of the transition metal oxide mesostructures during crystallization. Notably, mesoporous crystalline titania–carbon composites retained their hexagonal morphology up to 1000 °C. The carbon scaffold was subsequently removed by a second heat treatment in air at lower temperatures.

In this work, we employed the CASH method to generate ordered mesoporous crystalline γ-Al_2O_3–carbon composites and ordered mesoporous crystalline γ-Al_2O_3 structures. An amphiphilic structure-directing poly(isoprene)-*block*-poly(styrene)-*block*-poly(ethylene oxide) (PI-*b*-PS-*b*-PEO, ISO) triblock terpolymer was mixed with *n*-butanol and aluminum tri-*sec*-butoxide derived sols to form periodically ordered organic–inorganic hybrid mesostructures by solvent evaporation-induced self-assembly.[8] The ISO–Al_2O_3 hybrids were heated under an inert environment to induce γ-Al_2O_3 crystallization within the ISO-derived carbon matrix, retaining the ordered morphology, as well as stabilizing the γ-Al_2O_3 phase up to 1200 °C. The role of the carbon framework in controlling Al_2O_3 crystallization at the mesoscale was elucidated. The carbon matrix was subsequently removed by heating in air at 800 °C to obtain ordered mesoporous γ-Al_2O_3 structures with a well-defined pore size (~14 nm) and pore size distribution, as well as surface area and pore volume of approximately 200 $m^2\ g^{-1}$ and 0.7 $cm^3\ g^{-1}$, respectively.

Experimental

Chemicals

All chemicals were used as received. Anhydrous grades of tetrahydrofuran (≥99.9%, inhibitor-free), chloroform (≥99%, contains amylenes as stabilizer), *n*-butanol (99.8%) and aluminum tri-*sec*-butoxide (97%) were obtained from Sigma-Aldrich. 70 wt% nitric acid was obtained from Mallinckrodt Baker.

Synthesis of ISO-directed alumina (ISO–Al_2O_3) hybrids

The poly(isoprene)-*block*-poly(styrene)-*block*-poly(ethylene oxide) (ISO) triblock terpolymer with a molar mass of 38.3 kg mol^{-1} and polydispersity index of 1.07, containing 68.4 wt% PI, 18.0 wt% PS and 13.6 wt% PEO, was synthesized by sequential anionic polymerization as described elsewhere.[28,31,35] 0.05 g of ISO was dissolved in 1 g of tetrahydrofuran (THF) and 0.5 g of chloroform (3.2 wt% ISO solution). In a separate 20 mL scintillation vial (PTFE-lined cap), 1 g (3.9 mmol) of aluminum tri-*sec*-butoxide ($Al(O^sBu)_3$), 8 g of THF and 2.92 g (39.4 mmol) of *n*-butanol (*n*-BuOH) were added sequentially. The cloudy white suspension was stirred vigorously for homogenization. After 30 min of stirring, 0.511 mL (8.0 mmol) of 70 wt% nitric acid (HNO_3) was quickly added. (**Warning!** *Nitric acid reacts violently with organic solvents. Handle with caution.*) The mixture was stirred vigorously overnight (≥12 h) under ambient conditions to obtain a transparent colorless Al_2O_3 sol mixture. The water for hydrolysis was supplied by the HNO_3 source. Molar ratios of $Al(O^sBu)_3/HNO_3$, $Al(O^sBu)_3/H_2O$, and $Al(O^sBu)_3$/*n*-BuOH in the stock solution were approximately 1 : 2, 1 : 3, and 1 : 10, respectively. A 1.5 mL aliquot of the Al_2O_3 sol solution was added into the ISO solution and stirred for another 45 min. The resulting ISO–Al_2O_3 solution mixture was cast in a 5 mL PTFE beaker (VWR 89026-034) set on a glass Petri dish covered with a hemispherical glass dome, and heated at 50 °C on a hotplate under flowing nitrogen. A PTFE beaker containing 8–10 mL of anhydrous THF was placed next to the ISO–Al_2O_3 casting beakers to promote slow solvent evaporation. After 60–72 h of hotplate heating to evaporate most of the solvent, the ISO–Al_2O_3 hybrids were further aged in a vacuum oven at 130 °C overnight.

Synthesis of mesoporous crystalline alumina–carbon (MCA–C) composites

The ISO–Al_2O_3 hybrids were heated in a tube furnace under flowing nitrogen to 275 °C (1 h) and 600 °C (3 h) at a ramp rate of 1 °C min^{-1}, and subsequently raised to 1000–1200 °C (3–6 h) at a ramp rate of 5 °C min^{-1}. For thermal annealing at 1300 °C, ISO–Al_2O_3 hybrid samples were first heated under nitrogen to 275 °C (1 h) and 600 °C (3 h) at a ramp rate of 1 °C min^{-1}, and raised to 1200 °C (6 h) and 1300 °C (6 h) at a ramp rate of 5 °C min^{-1}.

Synthesis of mesoporous crystalline alumina (MCA–CASH) samples

To remove the carbon matrix, MCA–C composites were heated to 800 °C (2 h) at a ramp rate of 1 °C min^{-1} in static air unless described otherwise.

Characterization

A combination of bright-field transmission electron microscopy (TEM), scanning electron microscopy (SEM) and small-angle X-ray scattering (SAXS) was utilized to determine the morphology of the ISO-directed Al_2O_3 mesostructures.

TEM samples of ISO–Al_2O_3 hybrids were prepared by cryo-ultramicrotoming the films to a thickness of 50–80 nm using a Leica Ultracut UC7 cryo-ultramicrotome with a diamond knife at −60 °C. The microtomed sections were picked up from the surface of the water/dimethyl sulfoxide (4 : 6, v/v) mixture and subsequently placed on copper TEM grids. Bright-field TEM

micrographs were acquired using a FEI Tecnai 12 BioTWIN TEM operating at an accelerating voltage of 120 kV equipped with a Gatan Orius 1000 dual-scan CCD camera. SEM micrographs of uncoated MCA–C composites and Au–Pd coated all-Al_2O_3 MCA–CASH samples were acquired using a Zeiss LEO 1550 field emission SEM equipped with an in-lens detector.

SAXS measurements were conducted at the G1 beamline of the Cornell High Energy Synchrotron Source (CHESS). The G1 beamline setup consists of a multilayer monochromator with a beam energy of 10.5 keV and sample-to-detector distance of approximately 2.5 m. Part of the SAXS measurements was performed on a home-built beamline equipped with a Rigaku RU300 copper rotating anode generator, a set of orthogonal Franks focusing mirrors, and a phosphor-coupled CCD detector, as described elsewhere.[14] The two-dimensional (2D) SAXS patterns were azimuthally integrated around the beam center into 1D scattering intensity curves plotted against the scattering vector magnitude $q = 4\pi \sin\theta/\lambda$, where θ is half of the total scattering angle and λ is the X-ray wavelength.

Powder X-ray diffraction (PXRD) patterns were obtained on a Rigaku Ultima IV multipurpose X-ray diffraction system using Cu K_α radiation source and a D/Tex Ultra detector. Raman spectroscopy measurements were conducted on a Renishaw InVia confocal Raman microscope with a 785 nm excitation laser source. Thermogravimetric analysis (TGA) was performed using a TA Instruments Q500 instrument equipped with an autosampler and a Seiko Exstar TG/DTA 6200 thermal analyzer at heating rates of 1 to 5 °C min^{-1} under flowing air.

Nitrogen sorption measurements were performed using a Micromeritics ASAP 2020 surface area and porosity analyzer at −196 °C. The MCA–C composites and all-Al_2O_3 MCA–CASH samples were degassed at 150 °C under vacuum overnight (>8 h) prior to data acquisition. The specific surface areas were determined using the Brunauer–Emmett–Teller (BET) method[36,37] below 0.2 P/P_0. Pore size distributions were calculated using the Barrett–Joyner–Halenda (BJH) method.[36,38] Single point pore volumes were extracted at ~0.98–0.99 P/P_0.[36]

Results and discussion

ISO–Al_2O_3 hybrid mesostructures

The formation of ISO terpolymer-directed Al_2O_3 (ISO–Al_2O_3) hybrid mesostructures is shown schematically in Fig. 1. Aluminum tri-*sec*-butoxide ($Al(O^sBu)_3$) was employed as the Al source and mixed with *n*-butanol (*n*-BuOH) and nitric acid (HNO_3) in tetrahydrofuran (THF) as solvent to prepare the Al_2O_3 sol precursors. *n*-BuOH was chosen for two reasons. The ISO terpolymer dissolved well in the *n*-BuOH solvent.[30] Moreover, the longer *n*-butoxy ligands are expected to promote slower exchange reactions with $Al(O^sBu)_3$ (compared to shorter ethoxy or propoxy ligands) and reduce the overall sol–gel hydrolysis rates.[4,39] The molar ratio of $Al(O^sBu)_3$ to *n*-BuOH was set at 1 : 10. Small amounts of HNO_3 further lower the hydrolysis rate of Al_2O_3 sol precursors due to the large anion radius and weak complexation ability of NO_3^- to Al^{3+}.[21,25] The molar ratio of $Al(O^sBu)_3$ to HNO_3 was maintained at 1 : 2, similar to the work reported by Yan and co-workers.[21] We observed immediate white precipitation upon adding *n*-BuOH into the mixture of $Al(O^sBu)_3$ and THF and attributed this to alcoholysis.[4,39] The precipitates dissolved eventually resulting in a colorless transparent Al_2O_3 sol solution after adding HNO_3 to catalyze the hydrolysis reaction. An aliquot of Al_2O_3 sol solution was mixed with the ISO terpolymer dissolved in a solvent mixture of THF and chloroform (2 : 1, wt/wt), where the metal oxide sols selectively interacted with the hydrophilic PEO block by hydrogen bonds.[8,20,26,30] Periodically ordered ISO–Al_2O_3 hybrid mesostructures with long-range order were formed after solvent evaporation-induced self-assembly and aging in a vacuum oven. Structural properties of ISO-directed Al_2O_3 mesostructures were investigated using a combination of small-angle X-ray scattering, powder X-ray diffraction, electron microscopy, Raman spectroscopy, nitrogen sorption measurements and thermogravimetric analysis.

Fig. 2 presents the azimuthally integrated small-angle X-ray scattering (SAXS, Fig. 2a) and powder X-ray diffraction (PXRD, Fig. 2b) patterns of ISO–Al_2O_3 samples after aging at 130 °C, as well as thermal annealing at 1000 to 1200 °C. The SAXS pattern for the ISO–Al_2O_3 hybrid in Fig. 2a (black curve; sample (i)) displays the principal peak at q^* and other higher-order reflections at $(q/q^*)^2 = 1, 3, 4, 7, 9$, consistent with a hexagonal ($p6mm$) lattice and long-range order. Here the scattering vector magnitude, q, is defined by $q = 4\pi \sin\theta/\lambda$, with scattering angle 2θ and X-ray wavelength λ. The principal peak at $q^* = 0.164$ nm^{-1} corresponds to a cylinder-to-cylinder distance (d) of 44 nm (Table 1), where $d = 4\pi/(\sqrt{3}q^*)$. Interestingly, an inverse hexagonal lattice was observed in the ISO–Al_2O_3 hybrid samples as shown in the transmission electron microscopy (TEM) images in Fig. 3a and b, where PI/PS cylinders were most probably surrounded by the PEO/Al_2O_3 matrix. The TEM image in Fig. 3a exhibits multiple grain orientations of a hexagonal morphology. In some grains the hexagonally ordered cylinders can be observed head-on giving rise to the characteristic hexagonal honeycomb structure, while in others the cylinders are lying down thereby providing a cross-section similar to what is expected for a lamellar morphology. Thermogravimetric analysis (TGA, black curve) in Fig. 4a shows that the inorganic Al_2O_3 content constituted only ~22.5 wt% of the ISO–Al_2O_3 hybrid. We postulate *n*-BuOH acted as a

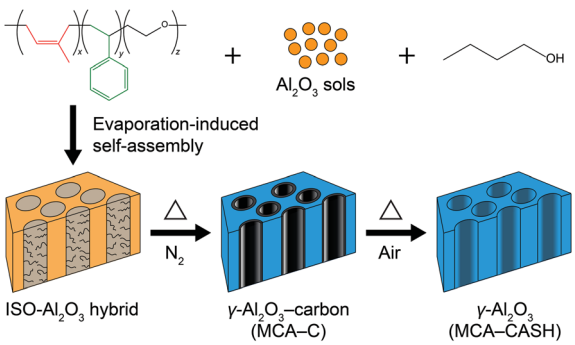

Fig. 1 Schematic illustration of ISO-directed ordered mesoporous crystalline γ-Al_2O_3 structures generated *via* CASH method (not drawn to scale).

co-solute[32–34] together with Al_2O_3 sols to swell the hydrophilic PEO block in ISO, yielding the inverse hexagonal hybrid mesostructure.

In order to explore *n*-BuOH as a co-solute, we utilized SAXS to characterize ISO–Al_2O_3 hybrids with different molar ratios of $Al(O^sBu)_3$ to *n*-BuOH whilst maintaining the same ISO to Al_2O_3 mass ratio for all samples (Fig. S1†). Reflections consistent with the hexagonal morphology were observed for hybrids with molar ratios of $Al(O^sBu)_3$ to *n*-BuOH between 1 : 5 and 1 : 10. However, the hexagonal morphology disappeared when the molar ratio was reduced to 1 : 15. For this molar ratio the broadening and shift of the principal peak to $q^* \approx 0.392$ nm^{-1} may be attributed to micellar aggregate formation.[26,30] This poorly ordered hybrid structure was not further characterized. In addition, the swelling of the PEO block by *sec*-BuOH released during the alcoholysis exchange reaction between $Al(O^sBu)_3$ and *n*-BuOH cannot be excluded either. Finally, in the absence of *n*-BuOH, inhomogeneous precipitation occurred upon addition of HNO_3 into a mixture of $Al(O^sBu)_3$ and THF that remained even after vigorous stirring for more than 48 h.

Ordered mesoporous γ-Al_2O_3–carbon composites and γ-Al_2O_3 structures

We employed the heating protocol of the CASH method to generate ordered mesoporous crystalline γ-Al_2O_3–carbon (MCA–C) composites and ordered mesoporous crystalline γ-Al_2O_3 (MCA) structures. Hereinafter, the samples are denoted as MCA-X-*Y*-*Z*, where X denotes either carbon *via* the letter "C" (after heating under nitrogen) or CASH (with carbon removed after heating in air), *Y* denotes the highest heating temperature, and *Z* indicates the holding duration at the highest temperature. A number of reactions occurred simultaneously during the first heat treatment under nitrogen. First, the PEO block decomposed and parts of the remaining terpolymer (PI/PS blocks) converted *in situ* into a rigid carbon matrix to support the inorganic Al_2O_3 mesostructure.[20,27] Consistent with earlier reports, Al_2O_3 crystallites then most likely nucleated and grew into wall material surrounded by the carbon matrix during crystallization.[15,18,20,23]

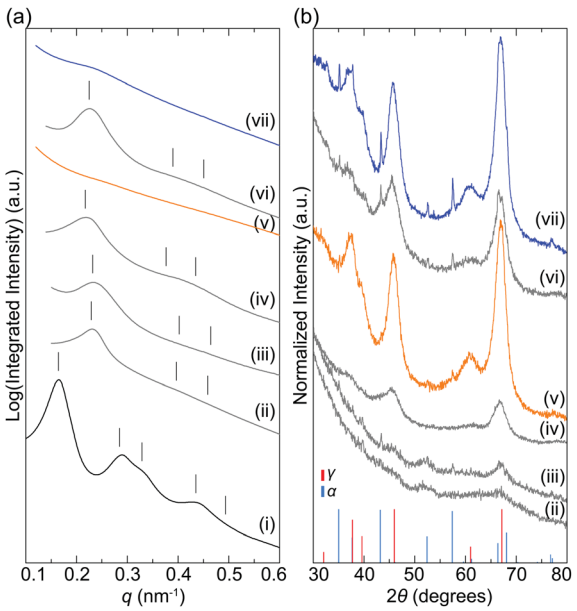

Fig. 2 (a) Azimuthally integrated SAXS, and (b) corresponding PXRD patterns of ISO–Al_2O_3 mesostructures after different heat treatments: (i) ISO–Al_2O_3 hybrid after aging at 130 °C (SAXS data only); (ii) MCA–C-1000-3 h; (iii) MCA–C-1100-3 h; (iv) MCA–C-1200-3 h; (v) MCA–CASH-1200-3 h; (vi) MCA–C-1200-6 h; (vii) MCA–CASH-1200-6 h. Tick marks in (a) indicate the expected SAXS reflections for a hexagonal (*p6mm*) lattice. PXRD peak markings and relative intensities for γ-Al_2O_3 (red, PDF 00-010-0425) and α-Al_2O_3 (sky blue, PDF 04-004-2852) are shown in (b). The data sets in (a) and (b) are offset vertically for clarity.

In comparison to the ISO–Al_2O_3 hybrids (black curve; sample (i)), the SAXS patterns of MCA–C composites (grey curves; samples (ii)–(iv) and (vi)) in Fig. 2a all display the principal peaks which broadened and shifted to higher *q* values (corresponding *d* values in Table 1) during thermal annealing from 1000 to 1200 °C under nitrogen, indicating mesostructure contraction up to 30% due to removal of the organic components. This is close to the macroscopic shape shrinkage of 34% for the black-colored MCA–C-1200 monolithic composites (Fig. S2†). The disappearance of the higher order reflections in the SAXS patterns indicate loss of some degree of long-range order that is typical during thermal annealing and attributed to Al_2O_3 crystallization-induced changes.[15,20,40] SEM micrographs in Fig. 3c–f and S3† corroborated that the MCA–C composites retained their hexagonal morphology from 1000–1200 °C under nitrogen.

PXRD patterns of MCA–C composites (grey curves; samples (ii)–(iv) and (vi)) in Fig. 2b show the crystallization evolution of mesostructured Al_2O_3 at different temperatures and holding durations under nitrogen. The MCA–C composites were transformed from the amorphous phase to γ-Al_2O_3 at 1000 °C held for 3 h (MCA–C-1000-3 h). The broad peaks suggest small γ-Al_2O_3 crystallites amid the predominant amorphous phase. Applying the Scherrer equation to the reflection at $2\theta = 67°$, the estimated size of the crystallites oriented to the (440) plane of γ-Al_2O_3 (PDF 00-010-0425) is 1–2 nm. The MCA–C composites became more crystalline with increasing temperatures. The γ-Al_2O_3 crystallites grew to 3–4 nm for thermal annealing at 1100 °C (MCA–C-1100-3 h) and 1200 °C (MCA–C-1200-3 h), when held for 3 h. We observed the onset of γ- to α-phase transformation in the MCA–C composites when the holding duration was extended to 6 h at 1200 °C as indicated by the appearance of new reflections consistent with α-Al_2O_3 phase (PDF 04-004-2852). The estimated α-Al_2O_3 crystallite size is 31 nm. Taking the area under the respective peaks as a measure for the number of scatterers, to first order the broad and intense PXRD reflections of γ-Al_2O_3 relative to the minority peaks of α-Al_2O_3 suggest that γ-Al_2O_3 is still by far the dominant phase under these conditions. When the annealing temperature was further increased to 1300 °C for 6 h, SAXS and SEM show that the MCA–C-1300-6 h composite mesostructure collapsed completely attributed to sintering of α-Al_2O_3 crystallites[15,21] (Fig. S4†). From PXRD, the MCA–C-1300-6 h composite was composed predominantly of the α-phase with an estimated crystallite size

Table 1 Structural characteristics of ISO-directed Al_2O_3 mesostructures

Designation	Cylinder-to-cylinder distance d,[a] nm	γ-Al_2O_3 crystallite size,[b] nm	α-Al_2O_3 crystallite size,[b] nm	Pore size,[c] nm	BET surface area, $m^2\ g^{-1}$ (micropore area,[e] $m^2\ g^{-1}$)	Pore volume,[d] $cm^3\ g^{-1}$ (micropore volume,[e] $cm^3\ g^{-1}$)
ISO–Al_2O_3 hybrid	44					
MCA–C-1000-3 h	32	1–2				
MCA–C-1100-3 h	31	3				
MCA–C-1200-3 h	33	3–4		17, 6, 2–3	167 (85)	0.15 (0.04)
MCA–C-1200-6 h	32	3–4	31	21, 6, 2–3	80 (33)	0.07 (0.02)
MCA–CASH-1200-3 h		4	32	14	197 (21)	0.70 (0.01)
MCA–CASH-1200-6 h		4	31	14	183 (28)	0.66 (0.01)

[a] Determined by SAXS. [b] Determined by PXRD. [c] Determined by BJH model from nitrogen sorption measurements. [d] Single point pore volume at ~0.98–0.99 P/P_0. [e] Determined by t-plot method from nitrogen sorption measurements.

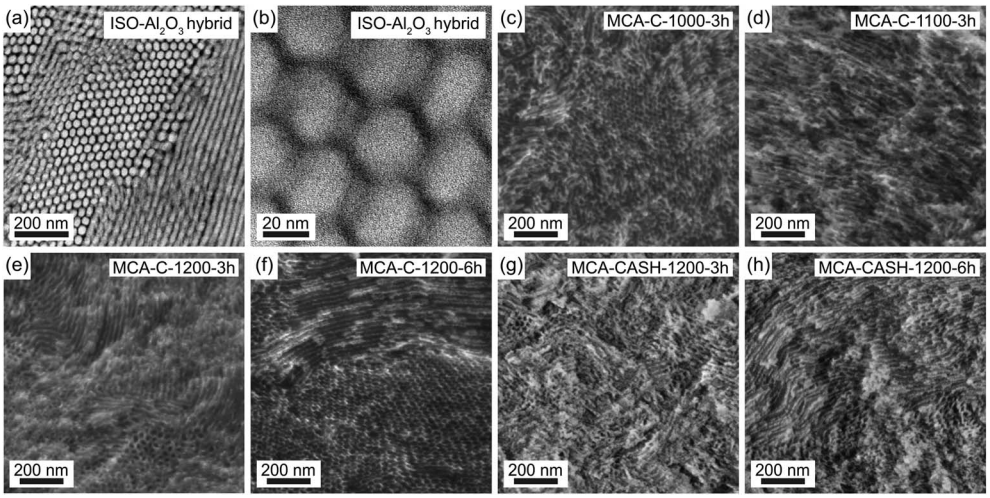

Fig. 3 (a and b) TEM micrographs of ISO–Al_2O_3 hybrid after aging at 130 °C. SEM micrographs of (c) MCA–C-1000-3 h; (d) MCA–C-1100-3 h; (e) MCA–C-1200-3 h; (f) MCA–C-1200-6 h; (g) MCA–CASH-1200-3 h; (h) MCA–CASH-1200-6 h.

of 36 nm. A new set of reflections observed in the PXRD pattern of MCA–C-1300-6 h composite further suggests reaction of the ISO-derived carbon with Al_2O_3 to form aluminum oxycarbide (Al_2OC, PDF 01-072-3584) during thermal annealing at 1300 °C for 6 h.

In order to remove the carbon matrix, MCA–C-1200 composites were subjected to a second heat treatment in (static) air at 800 °C for 2 h. The TGA profiles (compare grey and orange curves) in Fig. 4a demonstrate that the ISO-derived carbon from the first thermal annealing under nitrogen constituted almost 50 wt% of the MCA–C-1200 composites. Raman spectroscopy (grey curve) in Fig. 4b established the presence of ISO-derived carbon scaffold with the D and G-bands centered around 1300 and 1594 cm^{-1}, respectively.[20,41] After the second heat treatment in air, MCA–CASH-1200 monoliths appeared white, confirming removal of carbon (Fig. S2†). This was supported by the negligible mass loss (≤4%) in TGA (orange curve in Fig. 4a), as well as disappearance of both D and G-bands in the Raman spectrum (orange curve in Fig. 4b).

The SAXS patterns of the all-Al_2O_3 MCA–CASH-1200-3 h/6 h samples (orange and blue curves; samples (v) and (vii)) in Fig. 2a do not show well-defined reflections to allow assignment of a lattice structure. In contrast, representative SEM images in Fig. 3g and h (see also lower magnification images depicting larger areas of the samples in Fig. S5†) clearly demonstrate that the hexagonal morphology of the parent γ-Al_2O_3–carbon composite materials is retained after carbon removal. Aside from a small increase of the amount of α-Al_2O_3 relative to γ-Al_2O_3, PXRD reflections in Fig. 2b for both MCA–CASH-1200-3 h/6 h samples after carbon removal remained essentially unchanged to the corresponding MCA–C-1200-3 h/6 h composites, suggesting that the ordered Al_2O_3 mesostructures remained predominantly γ-phase.

Nitrogen sorption measurements established porosity in the MCA–C-1200-3 h/6 h composites and all-Al_2O_3 MCA–CASH-1200-3 h/6 h samples after carbon removal (Fig. 4c–f and Table 1). The nitrogen sorption isotherms of MCA–C-1200-3 h/6 h composites are type IV with H2 hysteresis, suggesting the pores were constricted at the pore openings or suffered from poor pore connectivity due to the high carbon content (Fig. 4c).[25,36] Specific surface areas of MCA–C-1200-3 h/6 h composites based on Brunauer–Emmett–Teller (BET)

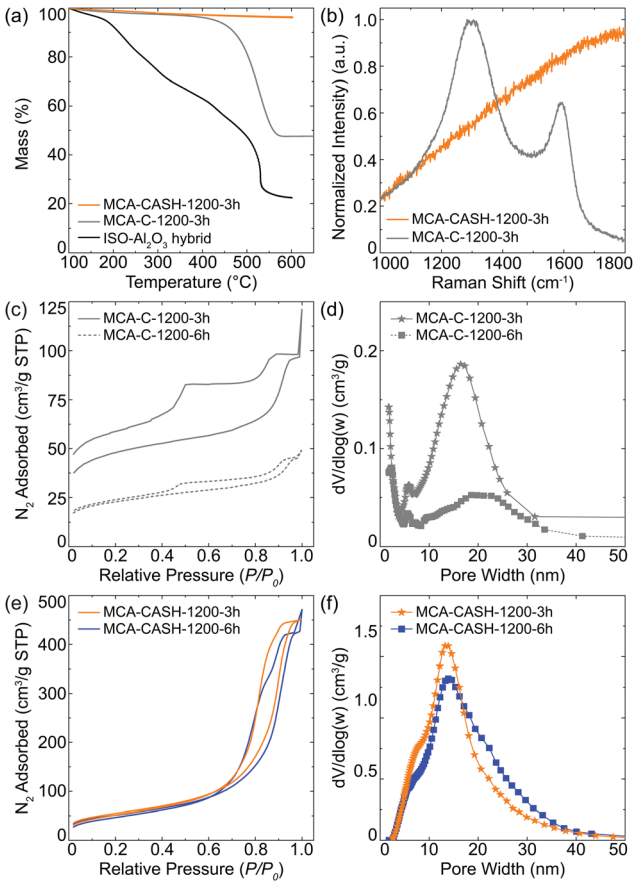

Fig. 4 (a) TGA data and (b) Raman spectra of ISO–Al_2O_3 hybrid (TGA data only), MCA–C-1200-3 h composite, and all-Al_2O_3 MCA–CASH-1200-3 h sample, as indicated. Nitrogen sorption isotherms and BJH pore size distributions of (c and d) MCA–C-1200-3 h/6 h composites and (e and f) all-Al_2O_3 MCA–CASH-1200-3 h/6 h samples after carbon removal, as indicated, respectively.

analysis[36,37] are 167 and 80 $m^2\ g^{-1}$, respectively. It is noted that microporosity contributed 41–51% to the total surface area. The difference in specific surface area for the MCA–C-1200-3/6 h composites supports the non-uniform distribution of ISO-derived carbon within the crystalline γ-Al_2O_3 mesostructures, resulting in constriction at the pore openings and poor pore connectivity.[25,36] Pore analysis based on the Barrett–Joyner–Halenda (BJH) method[36,38] shows a trimodal pore size distribution over the range of 2–30 nm (Fig. 4d). The largest pore sizes of MCA–C-1200-3 h/6 h composites are approximately 17 and 21 nm, respectively.

The nitrogen sorption isotherms for MCA–CASH-1200-3 h/6 h samples, *i.e.*, for all-Al_2O_3 samples after carbon removal, are type IV with H1 hysteresis (Fig. 4e).[25,36] The near vertical and sharp capillary condensation steps at approximately 0.9P/P_0 for both isotherms indicate high pore size uniformity and connectivity. The single peak of the pore size distribution centered at ~14 nm verified the vast improvement in the accessibility of mesopores (Fig. 4f). Moreover, specific surface areas increased to 197 and 183 $m^2\ g^{-1}$ for MCA–CASH-1200-3 h/6 h, respectively, which in addition to the SEM data sets further corroborate that the mesostructure is preserved after carbon removal. Contributions of the micropores to surface area and pore volume were reduced to less than 15% and 2%, respectively. From the pore volume of 0.7 $cm^3\ g^{-1}$ and γ-Al_2O_3 bulk density of 3.67 g cm^{-3}, the porosity for both all-Al_2O_3 MCA–CASH-1200-3 h/6 h samples is estimated to be around 70%. We postulate that a greater number of α-Al_2O_3 crystallites present in samples MCA–CASH-1200-6 h relative to MCA–CASH-1200-3 h resulted in the smaller specific surface area and wider pore size distribution.

Both SEM and nitrogen sorption measurement results clearly establish that the mesostructure is preserved after carbon removal. This raises the question why the SAXS patterns of all-Al_2O_3 MCA–CASH-1200-3 h/6 h samples (v and vii) in Fig. 2a do not show reflection peaks. We speculate the increased growth of γ-Al_2O_3 crystallites during heat treatment in air at 800 °C may have caused further roughening and size variations at the mesostructure interfaces, which becomes more dominant after removal of carbon that when present may smoothen the interfaces, leading to reduced scattering contrast factor and mesostructure domain correlations.[40]

Role of *in situ* carbon matrix

In previous literature, the typical onset crystallization temperatures for alkoxide sol–gel-derived amorphous Al_2O_3 conversions to γ-Al_2O_3 and α-Al_2O_3 phases are 750–800 °C and 1050–1100 °C, respectively.[4,21,29,39] However, in our present study, the solid-state phase transformation of MCA–C composites from amorphous to γ-Al_2O_3, and γ- to α-Al_2O_3 occurred at 1000 and 1200 °C, respectively; *i.e.*, the onset phase transformation temperatures were increased by 100–200 °C.

Above 600 °C under nitrogen, parts of the ISO terpolymer convert *in situ* into a rigid carbon matrix supporting the Al_2O_3 mesostructures during thermal annealing.[20,27] We postulate that Al and O atoms experienced reduced mobility at the mesostructured Al_2O_3 surfaces induced by the stabilizing effect of the surrounding carbon matrix.[3,5,15,20,24,40] The carbon matrix inhibits atomic migration of Al and O atoms, delaying nucleation most likely taking place at the surface[15] until the critical nucleus size of γ-Al_2O_3 (1–2 nm) is attained at 1000 °C. The γ-Al_2O_3 crystallites continue to grow (3–4 nm) with increasing temperature (up to 1200 °C) as the carbon matrix prevents sintering. However, γ-Al_2O_3 crystallites that are less protected by the carbon eventually sinter and transform into larger α-Al_2O_3 crystallites (>30 nm) at higher temperatures (≥1200 °C) and longer heating durations (≥3 h).[3,5]

In order to probe the reduced Al and O atomic mobility by the ISO-derived carbon, we prepared MCA–C composites by heating the ISO–Al_2O_3 hybrids to 1000 °C for 3 h under nitrogen (MCA–C-1000-3 h). The MCA–C-1000-3 h composites were then heated in air to remove the carbon matrix at a 1 °C min^{-1} ramp rate to 1000 °C and 1100 °C, respectively, where they were held subsequently for 1 h. This second heat treatment at 1000 °C (or 1100 °C) enabled further crystallization of MCA–C-1000-3 h composite after carbon removal. From SAXS (Fig. 5a) and PXRD (Fig. 5b) the broadening of the principal SAXS peak moving

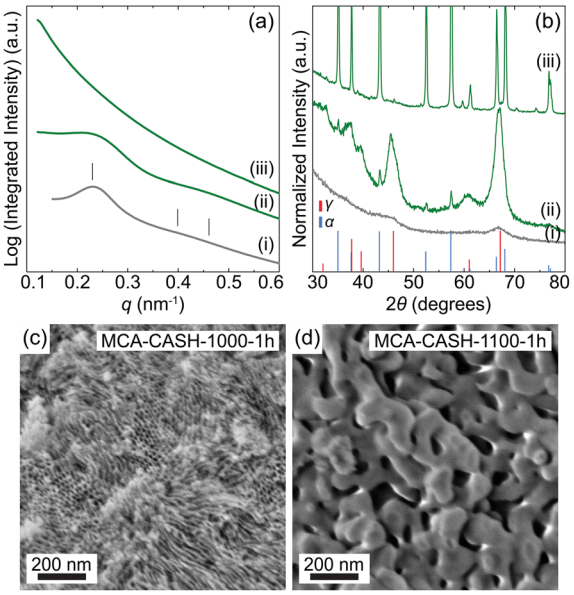

Fig. 5 (a) Azimuthally integrated SAXS and (b) corresponding PXRD patterns, of (i) MCA–C-1000-3 h composite; (ii) MCA–CASH-1000-1 h; (iii) MCA–CASH-1100-1 h, as well as (c and d) SEM micrographs of samples (ii) and (iii) as indicated. The tick marks in (a) indicate the expected SAXS reflections for the hexagonal morphology with $q^* = 0.230\ nm^{-1}$. PXRD peak markings and relative intensities for γ-Al_2O_3 (red, PDF 00-010-0425) and α-Al_2O_3 (sky blue, PDF 04-004-2852) are shown in (b). The data sets in (a) and (b) are offset vertically for clarity.

from MCA–C-1000-3 h composite to MCA–CASH-1000-1 h (*i.e.*, from sample (i, grey) to sample (ii, green) in Fig. 5a) was accompanied by the growth of γ-Al_2O_3 crystallites (from 1–2 nm to ~4 nm; see also Table 1) and transformation into some α-Al_2O_3 crystallites (~26 nm). SEM in Fig. 5c corroborated that the hexagonal morphology was retained under these conditions. The similarity in the PXRD patterns of MCA–CASH-1000-1 h (sample (ii, green) in Fig. 5b) and MCA–CASH-1200-6 h (sample (vii, blue) in Fig. 2b) supports the hypothesis that the carbon matrix in the latter delayed nucleation of Al and O atoms at the mesostructure surface by ~200 °C. When the MCA–C-1000-3 h composite was heated at 1100 °C in air, it transformed completely into the α-Al_2O_3 phase (crystallite size ~34 nm) resulting in the loss of hexagonal morphology as indicated by SAXS and SEM (MCA–CASH-1100-1 h, sample (iii) in Fig. 5a, b and d). This clearly demonstrates the importance of the carbon matrix in preserving the ordered mesoporous crystalline γ-Al_2O_3 structures and enhancing thermal stability up to 1200 °C, *vide supra*.

Conclusion

In summary, ordered mesoporous crystalline γ-Al_2O_3–carbon composites and ordered mesoporous crystalline γ-Al_2O_3 structures were synthesized by the combined assembly of soft and hard chemistries (CASH) approach. Periodically ordered ISO–Al_2O_3 mesophases were generated by evaporation-induced self-assembly of the structure-directing ISO terpolymer, *n*-butanol and aluminum tri-*sec*-butoxide derived sols. Thermal treatment in an inert environment converted parts of the ISO terpolymer into a rigid carbon matrix *in situ* to support γ-Al_2O_3 crystallization and preserved the structure by reducing Al and O atomic mobility and thus inhibiting nucleation and growth most likely at the surface. In particular, the ordered mesoporous crystalline γ-Al_2O_3–carbon composites exhibited high thermal stability up to 1200 °C. Ordered γ-Al_2O_3 mesostructures with uniform pore size (~14 nm) and high porosity (~70%) were obtained by removing the carbon matrix in a second heat treatment in air at 800 °C. To further improve mesostructure integrity, the carbon matrix could be removed at even lower temperatures such as in a moisture saturated environment. Future incorporation of metal oxide stabilizers[11,22] and platinum nanoparticles[24] into the ordered mesoporous γ-Al_2O_3 structures and γ-Al_2O_3–carbon nanocomposites may provide materials for high temperature catalysis applications.[1]

Acknowledgements

This work was supported by the National Science Foundation (NSF) Single Investigator Award (DMR-1409105). K.W.T. gratefully acknowledges the Singapore Energy Innovation Programme Office for a National Research Foundation graduate fellowship. T.N.H. was supported by the Swiss National Science Foundation with a Postdoctoral Fellowship. This work made use of research facilities at Cornell Center for Materials Research (CCMR) with support from the NSF Materials Research Science and Engineering Centers (MRSEC) program (DMR-1120296); Cornell High Energy Synchrotron Source (CHESS) which is supported by the NSF and the National Institutes of Health/National Institute of General Medical Sciences under NSF award DMR-1332208; Center for Energy and Sustainability at Cornell University; part of the SAXS data measurements is supported by DOE award DE-FG02-11ER16210. The authors acknowledge Dr J. Song and Dr M. Weathers of Cornell University for kind experimental assistance and helpful discussions.

References

1 T. Seki and M. Onaka, in *Advanced Nanomaterials*, ed. K. E. Geckeler and H. Nishide, Wiley-VCH Verlag GmbH & Co. KGaA, 2009, pp. 481–521.
2 Z. Zhang, R. W. Hicks, T. R. Pauly and T. J. Pinnavaia, *J. Am. Chem. Soc.*, 2002, **124**, 1592–1593.
3 L. L. Pérez, C. Alvarez-Galván, V. Zarubina, B. O. F. Fernandes and I. Melián-Cabrera, *CrystEngComm*, 2014, **16**, 6775–6783.
4 L. L. Pérez, S. Perdriau, G. ten Brink, B. J. Kooi, H. J. Heeres and I. Melián-Cabrera, *Chem. Mater.*, 2013, **25**, 848–855.
5 C.-P. Lin, S.-B. Wen and T.-T. Lee, *J. Am. Ceram. Soc.*, 2002, **85**, 129–133.
6 S. A. Bagshaw, E. Prouzet and T. J. Pinnavaia, *Science*, 1995, **269**, 1242–1244.
7 S. A. Bagshaw and T. J. Pinnavaia, *Angew. Chem., Int. Ed.*, 1996, **35**, 1102–1105.

8 M. Templin, A. Franck, A. D. Chesne, H. Leist, Y. Zhang, R. Ulrich, V. Schädler and U. Wiesner, *Science*, 1997, **278**, 1795–1798.
9 D. Zhao, J. Feng, Q. Huo, N. Melosh, G. H. Fredrickson, B. F. Chmelka and G. D. Stucky, *Science*, 1998, **279**, 548–552.
10 P. Yang, D. Zhao, D. I. Margolese, B. F. Chmelka and G. D. Stucky, *Nature*, 1998, **396**, 152–155.
11 W. Zhang and T. J. Pinnavaia, *Chem. Commun.*, 1998, 1185–1186.
12 F. Schüth, *Chem. Mater.*, 2001, **13**, 3184–3195.
13 T. Katou, B. Lee, D. Lu, J. N. Kondo, M. Hara and K. Domen, *Angew. Chem., Int. Ed.*, 2003, **42**, 2382–2385.
14 A. C. Finnefrock, R. Ulrich, G. E. S. Toombes, S. M. Gruner and U. Wiesner, *J. Am. Chem. Soc.*, 2003, **125**, 13084–13093.
15 B. L. Kirsch, E. K. Richman, A. E. Riley and S. H. Tolbert, *J. Phys. Chem. B*, 2004, **108**, 12698–12706.
16 M. Kuemmel, D. Grosso, C. Boissière, B. Smarsly, T. Brezesinski, P. A. Albouy, H. Amenitsch and C. Sanchez, *Angew. Chem., Int. Ed.*, 2005, **117**, 4665–4668.
17 K. Niesz, P. Yang and G. A. Somorjai, *Chem. Commun.*, 2005, 1986–1987.
18 Q. Liu, A. Wang, X. Wang and T. Zhang, *Chem. Mater.*, 2006, **18**, 5153–5155.
19 C. Boissière, L. Nicole, C. Gervais, F. Babonneau, M. Antonietti, H. Amenitsch, C. Sanchez and D. Grosso, *Chem. Mater.*, 2006, **18**, 5238–5243.
20 J. Lee, M. C. Orilall, S. C. Warren, M. Kamperman, F. J. DiSalvo and U. Wiesner, *Nat. Mater.*, 2008, **7**, 222–228.
21 Q. Yuan, A.-X. Yin, C. Luo, L.-D. Sun, Y.-W. Zhang, W.-T. Duan, H.-C. Liu and C.-H. Yan, *J. Am. Chem. Soc.*, 2008, **130**, 3465–3472.
22 S. M. Morris, P. F. Fulvio and M. Jaroniec, *J. Am. Chem. Soc.*, 2008, **130**, 15210–15216.
23 Z. Wu, Q. Li, D. Feng, P. A. Webley and D. Zhao, *J. Am. Chem. Soc.*, 2010, **132**, 12042–12050.
24 J. Xu, A. Wang, X. Wang, D. Su and T. Zhang, *Nano Res.*, 2011, **4**, 50–60.
25 S. M. Grant and M. Jaroniec, *J. Mater. Chem.*, 2012, **22**, 86–92.
26 X. Jiang, N. Suzuki, B. P. Bastakoti, K. C.-W. Wu and Y. Yamauchi, *Chem.–Asian J.*, 2012, **7**, 1713–1718.
27 T. Lunkenbein, D. Rosenthal, T. Otremba, F. Girgsdies, Z. Li, H. Sai, C. Bojer, G. Auffermann, U. Wiesner and J. Breu, *Angew. Chem., Int. Ed.*, 2012, **51**, 12892–12896.
28 M. Stefik, S. Wang, R. Hovden, H. Sai, M. W. Tate, D. A. Muller, U. Steiner, S. M. Gruner and U. Wiesner, *J. Mater. Chem.*, 2012, **22**, 1078–1087.
29 L. L. Pérez, V. Zarubina, H. J. Heeres and I. Melián-Cabrera, *Chem. Mater.*, 2013, **25**, 3971–3978.
30 K. W. Tan, D. T. Moore, M. Saliba, H. Sai, L. A. Estroff, T. Hanrath, H. J. Snaith and U. Wiesner, *ACS Nano*, 2014, **8**, 4730–4739.
31 S. W. Robbins, H. Sai, F. J. DiSalvo, S. M. Gruner and U. Wiesner, *ACS Nano*, 2014, **8**, 8217–8223.
32 F. Kleitz, S. H. Choi and R. Ryoo, *Chem. Commun.*, 2003, 2136–2137.
33 F. Kleitz, L. A. Solovyov, G. M. Anilkumar, S. H. Choi and R. Ryoo, *Chem. Commun.*, 2004, 1536–1537.
34 T.-W. Kim, F. Kleitz, B. Paul and R. Ryoo, *J. Am. Chem. Soc.*, 2005, **127**, 7601–7610.
35 J. Allgaier, A. Poppe, L. Willner and D. Richter, *Macromolecules*, 1997, **30**, 1582–1586.
36 M. Kruk and M. Jaroniec, *Chem. Mater.*, 2001, **13**, 3169–3183.
37 S. Brunauer, P. H. Emmett and E. Teller, *J. Am. Chem. Soc.*, 1938, **60**, 309–319.
38 E. P. Barrett, L. G. Joyner and P. P. Halenda, *J. Am. Chem. Soc.*, 1951, **73**, 373–380.
39 L. Ji, J. Lin, K. L. Tan and H. C. Zeng, *Chem. Mater.*, 2000, **12**, 931–939.
40 S. C. Warren, L. C. Messina, L. S. Slaughter, M. Kamperman, Q. Zhou, S. M. Gruner, F. J. DiSalvo and U. Wiesner, *Science*, 2008, **320**, 1748–1752.
41 A. C. Ferrari and J. Robertson, *Phys. Rev. B: Condens. Matter Mater. Phys.*, 2000, **61**, 14095–14107.